BPURS DELIVERABLE
A WEAK GRAVITATIONAL LENSING REVIEW

FREDRICK WILLIAM HIGH

ABSTRACT. Gravitational lensing arises from the curvature of spacetime, which itself is a result of the presence of energy and momentum a la Einstein's Equation. Einstein's General Theory of Relativity predicts that inhomogeneous distribution of matter deflects a nearby photon's trajectory. We derive the result that Einstein himself first arrived at. Nowadays, the study of gravitational lensing's weakest regime is maturing rapidly as a result of the advanced state of land- and space-based imaging technology. Weak lensing provides one of the first direct measures of dark matter in the sky. This article reviews the theory and conventions of weak gravitational lensing, summarizes three prominent methods for detecting it, and presents some initial data from our own weak lensing studies in the Great Observatories Origins Deep Survey (GOODS) images. This review is intended for advanced undergraduates in physics or closely related fields.

1. Review of the Theory

Einstein's General Theory of Relativity fully describes the deflection of light by a gravitational potential. We call this gravitational lensing because of the natural analogy to classical lensing systems. However, most of nature's gravitational lenses are far from the idealized lenses we are familiar with. Light behaves in a gravitational potential gradient the way it would when passing through substances of varying indeces of refraction. The analogy, in fact, is made even closer when we identify an effective index of refraction in the case of gravity.

1.1. A General Relativistic Derivation of the Deflection of Light by Gravity.

The General Relativistic analogy to Poisson's equation is called the Einstein Equation, written elegantly in a second order tensor equation as

$$\mathbf{G} = 8\pi G\mathbf{T}. \tag{1.1}$$

The lefthand side bears close resemblance to the second order derivative on the classical potential field Φ from Newton's theory. In fact, $\mathbf{G}$ represents a manner of second order derivatives on the spacetime metric, which is the corresponding "field" in GR. The metric is essentially the coordinate system we use to label or index events in space and time. As we know, a second order derivative tells us something about the curvature of its operand. Likewise, $\mathbf{G}$ tells us about the curvature of the metric, which we can naturally interpret as the curvature of spacetime itself.

The righthand side of (1.1) contains the $4\pi G$ from the Poisson Eqation but with an extra factor of two. G here is the Newtonian gravitational constant, as it must be if (1.1) is to reduce to the classical theory in the nonrelativistic limits. And finally, $\mathbf{T}$ is the energy-momentum tensor from classical theory. Whereas the mass density ρ is the source of the gravitational field in Newton's theory, $\mathbf{T}$ is the source of spacetime curvature in General Relativity. Amazingly, the source of spacetime curvature, which gives rise to gravitation, is not only mass but momentum and energy as well. $\mathbf{T}$ contains this information.

Date: May 11, 2004.

If we assume speeds $v \ll c$, where c is the speed of light, and weak energy-momentum disribution[1] , then we can use classical perturbative methods to approximate the Einstein Equation. The resulting field equation is the Poisson Equation, as it must be.

Given spherical symmetry in four dimensional spacetime, Schwarzschild's metric solves Einstein's Equation generally. Four dimensional spherical symmetry also gives rise to two useful Killing vectors, which reflect the symmetries of the metric. These Killing vectors are

$$\xi = \begin{pmatrix} 1 & 0 & 0 & 0 \end{pmatrix}, \tag{1.2}$$

$$\eta = \begin{pmatrix} 0 & 0 & 0 & 1 \end{pmatrix}. \tag{1.3}$$

ξ arises from the time independence of the Schwarzschild metric, and η arises from the azimuthal angle ϕ independence. In units of $c = G = 1$, or *geometrized units*, the conserved quantities for any geodesic in Schwarzschild geometry are

$$e \equiv -\xi \cdot \mathbf{u} = \left(1 - \frac{2M}{r}\right)\frac{\mathrm{d}t}{\mathrm{d}\lambda}, \tag{1.4}$$

$$l \equiv \eta \cdot \mathbf{u} = r^2 \sin^2\theta \frac{\mathrm{d}\phi}{\mathrm{d}\lambda}, \tag{1.5}$$

where λ is some affine parameter for the body's trajectory in spacetime and $\mathbf{u}$ is the body's four-velocity in its general form. We may restrict our analysis to the $\theta = \pi/2$ plane because the body will remain there for unperturbed motion. e is the GR analog of the total energy E for orbital motion in Newtonian dynamics, and l is the analog of the Newtonian angular momentum, both conserved quantities in Newtonian orbital motion.

We require for a photon's null geodesic that

$$\mathbf{u} \cdot \mathbf{u} = g_{\mu\nu} u^\mu u^\nu = g_{\mu\nu} \frac{\mathrm{d}x^\mu}{\mathrm{d}\lambda}\frac{\mathrm{d}x^\nu}{\mathrm{d}\lambda} = 0. \tag{1.6}$$

This is by construct of the metric. In the present case we only have $\mu, \nu = \{t, r, \phi\}$, the metric is diagonal, and we can plug in from (1.4) and (1.5) to get

$$-\left(1 - \frac{2M}{r}\right)\left(\frac{\mathrm{d}t}{\mathrm{d}\lambda}\right)^2 + \left(1 - \frac{2M}{r}\right)\left(\frac{\mathrm{d}r}{\mathrm{d}\lambda}\right)^2 + r^2\left(\frac{\mathrm{d}\phi}{\mathrm{d}\lambda}\right)^2 = 0. \tag{1.7}$$

We can eliminate the derivatives from the first and last terms on the lefthand side in favor of the constants e and l using (1.4) and (1.5). This gives

$$-\left(1 - \frac{2M}{r}\right)^{-1} e^2 + \left(1 - \frac{2M}{r}\right)^{-1}\left(\frac{\mathrm{d}r}{\mathrm{d}\lambda}\right)^2 + \frac{l^2}{r^2}. \tag{1.8}$$

We can put this in the simple and illuminating form

$$\frac{e^2}{l^2} = \frac{1}{l^2}\left(\frac{\mathrm{d}r}{\mathrm{d}\lambda}\right)^2 + \frac{1}{r^2}\left(1 - \frac{2M}{r}\right). \tag{1.9}$$

It turns out that $|l/e|$ reduces to something useful. Dividing (1.5) by (1.4) at $r >> 2MG/c^2$, we have

$$\left|\frac{l}{e}\right| \approx r^2 \frac{\mathrm{d}\phi}{\mathrm{d}t}. \tag{1.10}$$

At large r we have $\phi \approx b/r$, where b is the impact parameter, or the lateral distance between the photon's trajectory and the location of the source mass. We also have

[1]Weak energy-momentum distribution is itself defined by velocities well below the speed of light and also by

$$\frac{GM}{c^2 b} \ll 1,$$

where b is the impact parameter of the light ray, defined as the lateral distance of the light ray's trajectory to the source.

$\mathrm{d}r/\mathrm{d}t \approx -c$ because the velocity of the photon at large r is directed almost entirely radially inward. This gives

$$\frac{\mathrm{d}\phi}{\mathrm{d}t} = \frac{\mathrm{d}\phi}{\mathrm{d}r}\frac{\mathrm{d}r}{\mathrm{d}t} = \frac{d}{r^2}. \tag{1.11}$$

This yields finally

$$\boxed{\left|\frac{l}{e}\right| = b.} \tag{1.12}$$

In light of this result and the definition of the effective potential for photon orbits,

$$V_{\mathrm{eff}}(r) \equiv \frac{1}{r^2}\left(1 - \frac{2M}{r}\right), \tag{1.13}$$

we now have greater insight on (1.9) if we write it as

$$\boxed{\frac{1}{b^2} = \frac{1}{l^2}\left(\frac{\mathrm{d}r}{\mathrm{d}\lambda}\right)^2 + V_{\mathrm{eff}}.} \tag{1.14}$$

We are interested in the angle through which the source mass deflects the photon, which approaches from infinity with impact parameter b and arrives at our location, also at infinity. We can get this by finding an expression for $\mathrm{d}r/\mathrm{d}\phi$ and integrating from the radius of closest approach to infinity[2]. We can find the expression we want by eliminating $1/l^2$ from (1.14) using (1.5) and solving for our desired quantity. This gives

$$\frac{\mathrm{d}r}{\mathrm{d}\phi} = \pm r^2\left(\frac{1}{b^2} - V_{\mathrm{eff}}\right)^{1/2}, \tag{1.15}$$

where the sign indicates whether the photon is approaching or retreating from the source mass. Because the trajectory is symmetric about the axis through the radius of closest approach r_0, we can find our angle by solving integrating

$$\Delta\phi = 2\int_{r_0}^{\infty}\frac{\mathrm{d}r}{r^2}\left[\frac{1}{b^2} - \frac{1}{r^2}\left(1 - \frac{2M}{r}\right)\right]^{-1/2}. \tag{1.16}$$

We can determine the radius of closest approach using (1.14) by noting that the derivative vanishes when the photon reaches this point, yielding $1/b^2 = V_{\mathrm{eff}}(r_0)$. r_0 is then a root of the equation

$$\frac{1}{b^2} = \frac{1}{r^2}\left(1 - \frac{2M}{r}\right). \tag{1.17}$$

We now introduce a natural change of variable

$$u = b/r, \tag{1.18}$$

which gives a new integral

$$\Delta\phi = \int_0^{u_0}\mathrm{d}u\left[1 - u^2\left(1 - \frac{2M}{b}u\right)\right]^{-1/2} \tag{1.19}$$

$$= 2\int_0^{u_0}\mathrm{d}u\left(1 - \frac{2M}{b}u\right)^{-1/2}\left[\left(1 - \frac{2M}{b}u\right)^{-1} - u^2\right]^{-1/2} \tag{1.20}$$

u_0 here is a root of the bracketed expression. We have written the latter expression in this form because we wish to expand the integrand in powers of $2M/b$, which we define to be small. The result is

$$\Delta\phi = 2\int_0^{u_0}\mathrm{d}u\frac{1 + (M/b)u}{[1 + (2M/b)u - u^2]^{1/2}}. \tag{1.21}$$

[2]Because the orbit of the photon is symmetric about the line of closest approach, there is no danger of ambiguity as to *which* $r = \infty$ we are talking about.

u_0 is still a root of the bracketed expression. This integral evaluates to

$$\Delta\phi = \pi + \frac{4M}{b}. \tag{1.22}$$

It is convenient to find the angle of deflection $\delta\phi = \Delta\phi - \pi$. After replacing c, $G \neq 1$, this gives us our final result for the deflection of a photon outside a spherically symmetric mass,

$$\boxed{\delta\phi = \frac{4GM}{c^2 b}.} \tag{1.23}$$

This result is twice that rederived in 1911 by Einstein himself from the Newtonian theory. The discrepancy results from the postulate that spacetime is curved.

1.2. **Weak Lensing Conventions.** Gravitational lensing in its weak regime has become a viable field of study of its own right in the last couple decades. To become involved in this study, one must become familiar with the conventions that have come into use. To begin with we write down what every undergraduate knows already from courses on electrostatics and classical gravity: Poisson's Equation.

$$\nabla^2\Phi = 4\pi G\rho, \tag{1.24}$$

where we identify the Laplacian's argument Φ as the Newtonian gravitational potential, G as Newton's gravitational constant, and ρ as the three dimensional mass density. With the usual physical constraints on Φ, e.g., continuity and identification of a zero value somewhere, this equation uniquely determines the potential given a mass distribution.

We can collapse one of the dimensions of this equation by projecting all quantities onto the xy-plane. Projection is an integration, and we define the two dimensional projected potential and mass density as

$$\Psi = \int \Phi \mathrm{d}z, \tag{1.25}$$

$$\Sigma = \int \rho \mathrm{d}z, \tag{1.26}$$

respectively. One may visualize this operation as taking some three dimensional mass distribution, summing the mass densities along all lines of constant x and y, and placing the summed mass at $z = 0$.

Note that the resultant Σ is not simply z-independent. In other words, this is a sheet mass and not some mass density field that extends in three dimensions but symmetrically in z. Therefore, in introducing the two dimensional Poisson Equation,

$$\nabla^2\Psi = 4\pi G\Sigma, \tag{1.27}$$

we imply the two dimensional Laplacian, $\nabla^2 = \partial_x^2 + \partial_y^2$. Afterall, this equation results when we integrate the z variable out altogether. This point is subtle. In electrostatics, we sometimes seek the *three dimensional* electric potential given a *two dimensional* sheet of charge. Naturally, we may do so in gravito-statics as well, but that is not what we are doing here. Instead, we are concerned with the gravitational potential only in the plane of the sheet mass and after projection.

We can define a critical sheet mass density as

$$\Sigma_c = \frac{c^2}{4\pi G}\frac{D_s}{D_d D_{ds}}, \tag{1.28}$$

where the D's are angular diameter distances[3]. Σ_c allows us to define a dimensionless sheet mass density

$$\kappa = \Sigma/\Sigma_c \tag{1.29}$$

[3]see Hogg 2000 for a description of this measure of distance and Kuijken 2003 for motivation for Σ_c.

and a modified two dimensional projected gravitational potential

$$\psi = \Psi / 2\pi G \Sigma_c, \tag{1.30}$$

the latter of which yields a dimensionless quantity when operated on by the two dimensional Laplacian. This is evident in our new Poisson Equation

$$\boxed{\nabla^2 \psi = \kappa.} \tag{1.31}$$

Again, we arrive at this eqation by (1) collapsing a dimension and (2) making the equation dimensionless by dividing by critical quantities.

We can now define the Jacobian matrix

$$A_{ij} = \delta_{ij} - \psi_{,ij}, \tag{1.32}$$

where the comma denotes partial differentiation with respect to the ith and jth coordinate and $i,\ j = \{1, 2\}$. Explicitly,

$$A = \begin{pmatrix} 1 - \psi_{,11} & -\psi_{,12} \\ -\psi_{,21} & 1 - \psi_{,22} \end{pmatrix} \tag{1.33}$$

$$= \begin{pmatrix} 1 - [\frac{1}{2}(\psi_{,11} + \psi_{,22}) + \frac{1}{2}(\psi_{,11} - \psi_{,22})] & -\psi_{,12} \\ -\psi_{,21} & 1 - [\frac{1}{2}(\psi_{,11} + \psi_{,22}) - \frac{1}{2}(\psi_{,11} - \psi_{,22})] \end{pmatrix} \tag{1.34}$$

$$= \begin{pmatrix} 1 - \kappa - \gamma_1 & -\gamma_2 \\ -\gamma_2 & 1 - \kappa + \gamma_1 \end{pmatrix}. \tag{1.35}$$

Clearly we have used

$$\kappa = \nabla^2 \psi = \psi_{,11} + \psi_{,22} \tag{1.36}$$

and defined

$$\gamma_1 \equiv \frac{1}{2}(\psi_{,11} - \psi_{,22}), \qquad \gamma_2 \equiv \psi_{,12} = \psi_{,21}, \tag{1.37}$$

where the latter equality holds from Clairaut's Theorem. It turns out that γ_i are the components of the shear of an image and κ is equal to the convergence.

Conventially, we define A^{-1} as the magnification matrix with the property that

$$M = \det A^{-1} = \frac{1}{\det A} = [(1 - \kappa)^2 - \gamma_1^2 - \gamma_2^2]^{-1}. \tag{1.38}$$

M is called the magnification. Weak gravitational lensing is defined by the conditions $\kappa \ll 1$ and $|\gamma_i| \ll 1$. We find the first order binomial expansion of M to be

$$M_{WL} = 1 + 2\kappa. \tag{1.39}$$

2. Methods in Weak Lensing Detection

To detect weak lensing in images, three methods have become prominent in recent years. They resemble each other closely in that they all involve measuring galaxy shapes, deconvolving and correcting for distortion, and statistically correlating the corrected galaxy shapes. We present here a detailed summary of the KSB method, and more concise reviews of the RRG and Shapelets methods of weak lensing detection.

2.1. **KSB.** Kaiser, Squires and Broadhurst [KSB] (hereafter KSB) put forth the simplest of the three methods summarized here. Their algorithm consists of four essential steps. Given an image they propose that we

(1) find the sources,
(2) measure the source shapes,
(3) measure the Point Spread Function (PSF),
(4) and estimate the shear.

2.1.1. *Find the sources.* First we find the galaxies and stars in our image. To locate objects KSB suggest simply detecting peaks in the smoothed image. The smoothing radii should be made to vary in order to maximize the significance ν at each peak, where ν is defined as the signal-to-noise ratio, $\nu \equiv S/N$. In fact, the smoothing radius that maximizes the significance at a peak can also provide a good preliminary estimate of the object extent σ. This is especially true for sources with Gaussian intensity profiles, but KSB shows qualitatively that this is generally useful nonetheless.

After peaks are detected and their optimum significances are determined from variable smoothing radii, a large gap becomes evident between real sources and spurious source detections attributable to noise peaks. We identify this gap and eliminate all sources with significance below this level. We may also find "composite sources," which are sources that overlap to some extent. We may easily detect these and choose to throw them out in order to make clean subsequent shape measurements.

2.1.2. *Measure the source shapes.* After we locate the peaks and determine whether each is a star or a galaxy, we then measure the shape of each galaxy. KSB are interested in only a few shape parameters. They use what Blanford et al. 1991 [1] call the polarization $\mathbf{e} = (e_1, e_2)$. $\mathbf{e}$ is a normalized measure of the ellipticity of an object. Namely, e_1 quantifies the amount of elongation in the horizontal direction and e_2 the elongation at 45°. Each component can take on values between -1 and 1, where a positive value represents stretch and a negative value represents squash. For example, a horizontal ellipse has $e_2 = 0$ and $0 < e_1 < 1$, and a vertical lying ellipse still has $e_2 = 0$ but $-1 < e_1 < 0$. An ellipse oriented at $+45°$ from the horizontal has $e_1 = 0$ and $0 < e_2 < 1$, and an ellipse at an angle of $-45°$ has $e_1 = 0$ and $-1 < e_2 < 0$.

From this description and our present knowledge of ellipses, some features of the polarization become obvious. If we define the angle of inclination of an ellipse as α, we can show that $\mathbf{e}$ is symmetric on rotation by 180°, or $\mathbf{e}(\alpha) = \mathbf{e}(\alpha + \pi)$. This reflects the fact that putting a negative sign in front of an ellipticity simply rotates it by 90°, and is a feature of any spin two quantity.

Ellipticity interests us because we may postulate that, in the absence of weak lensing, a local ensemble of galaxies has randomly distributed polarizations. This appears as a null average over a population. Weak lensing correlates polarizations locally in an image, so ideally the only error in our lensing measurements are statistical and thus quantifiable. However, we find that other effects such as an anisotropic PSF also correlate object polarizations on the same order of magnitude as weak lensing. We discuss this in §2.1.3.

Before arriving at the polarization we first find the source barycenter θ^c. This is defined to be the location of the weighted first order moment or "center of intensity" of the source,

$$\theta_i^c \equiv \frac{I_i'}{I} \equiv \frac{\int \mathrm{d}^2\theta' \theta_i' W((\theta' - \theta^c)^2/\sigma^2) i(\theta')}{\int \mathrm{d}^2\theta' W(\theta' - \theta^c) i(\theta')}, \tag{2.1}$$

where θ' are the original coordinates, normally with origin at some corner of the image, $i(\theta)$ is the intensity at location θ in the image of the source, and W is some square integrable weight function with extent σ. W is normally chosen to be a Gaussian. If we introduce a change of coordinates $\theta_i = \theta_i' - \theta_i^c$ such that the new, unprimed origin is located at θ_i^c, then we can arrive at a new, useful expression by plugging into (2.1),

$$0 = \int \mathrm{d}^2\theta' (\theta_i' - \theta_i^c) W((\theta' - \theta^c)^2/\sigma^2) i(\theta'). \tag{2.2}$$

We can iteratively solve (2.2) to find θ_i^c and to optimize σ, which is taken to be the extent of the source following Hoekstra et al. 1998 [HFKS].

Of the weighted, low order multipole moments in the unprimed coordinate system,

$$I \equiv \int \mathrm{d}^2\theta W(\theta/\sigma^2) i(\theta), \tag{2.3}$$

$$I_i \equiv \int \mathrm{d}^2\theta \theta_i W(\theta/\sigma^2) i(\theta) \equiv 0, \tag{2.4}$$

$$I_{ij} \equiv \int \mathrm{d}^2\theta \theta_i \theta_j W(\theta/\sigma^2) i(\theta), \tag{2.5}$$

we have only to find the monopole and quadrupole terms[4]. We may wish to normalize the quadrupole moment as

$$J_{ij} \equiv I_{ij}/I, \tag{2.9}$$

but we shall find this unnecessary at the moment.

Finally, we calculate the source polarizations as

$$\boxed{e_1 = (I_{11} - I_{22})/T, \qquad e_2 = 2I_{12}/T,} \tag{2.10}$$

where the trace $T \equiv I_{11} + I_{22}$.

It is crucial to weight the moments in the KSB method with well defined functions. This will become evident in §2.1.3 when we show KSB's results for PSF deconvulution. In a word, the deconvolution can be intractable without a well defined, analytic weight. Figure 1 shows histograms our own polarization measurements of sources in one of the GOODS images. These are yet unweighted by an analytical function, and this represents our next step in measuring shapes.

2.1.3. *Measure the PSF.* After we locate sources and measure their shapes, we measure and correct for the PSF. Typically we measure the PSF by locating stars in the field, measuring their polarizations as in §2.1.2, and interpolating between the stars using low order polynomial approximations. First we define the relation between the polarization and the PSF.

The anisotropic part of the PSF perturbs source polarization to first order as

$$e_i^{\mathrm{obs}} = e_i^{\gamma} + \delta e_i^{\mathrm{sm}} \tag{2.11a}$$

$$= e_i^{\gamma} + P_{ij}^{\mathrm{sm}} p_j. \tag{2.11b}$$

e_i^{γ} are the pure gravitationally lensed polarizations, that is, those polarizations before the PSF takes effect. KSB dub P^{sm} the "smear polarizability" tensor, as it tells us to what extent the anisotropic component of the PSF affects the source polarization to linear order. p_i are the polarization components of the anisotropic component of the PSF. We first define the anisotropic part p of the PSF P as the kernel in the convolution of the isotropic part P^{iso} in the relation

$$P(\theta) = \int \mathrm{d}^2\theta' p(\theta') P^{\mathrm{iso}}(\theta - \theta'). \tag{2.12}$$

[4]In practice, these integrals become sums,

$$I \equiv \sum_{i,j \in S} W(\theta/\sigma^2) i(\theta), \tag{2.6}$$

$$I_i \equiv \sum_{i,j \in S} \theta_i W(\theta/\sigma^2) i(\theta) \equiv 0, \tag{2.7}$$

$$I_{ij} \equiv \sum_{i,j \in S} \theta_i \theta_j W(\theta/\sigma^2) i(\theta). \tag{2.8}$$

where θ_i are expressed here in pixels. Hence $\Delta\theta_i = 1$ here. S denotes some subset of the image, normally a circular aperture a few times the extent of the source.

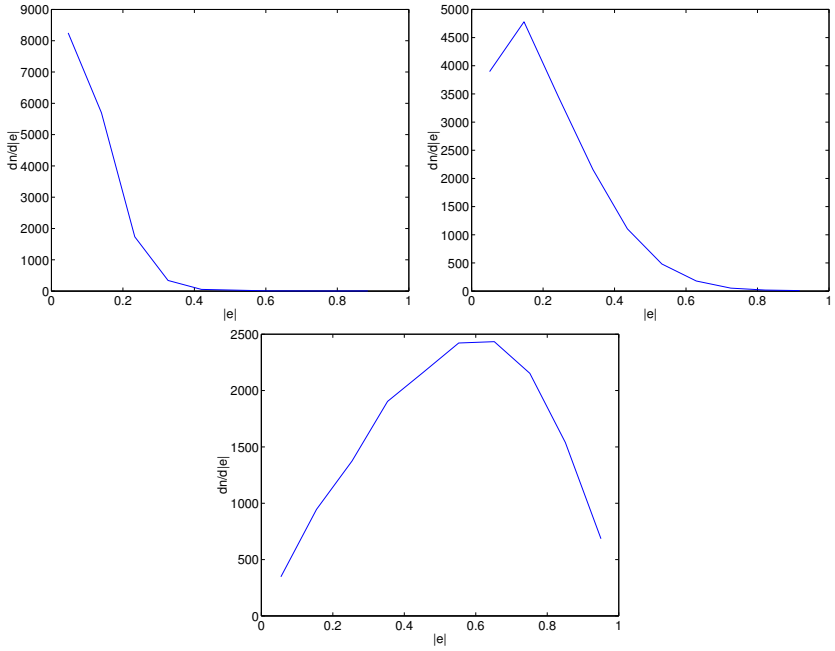

FIGURE 1. Histograms of the polarization magnitudes in GOODS HDF-N, version 1.0, tile 33, i-band. There are about 8000 sources in this image. Clockwise from the top left: (1) Polarizations of the raw source images with circular apertures. The sources appear overwhelmingly round, signified by a small e. (2) Polarization of the same sources after setting all pixels below the noise rms to zero. The mean average polarization magnitude increases, so this scheme effectively amplifies the polarization signal, meaning their ellipticities are more evident. (3) Polarization of the sources from (2), but with all pixels not contiguous with the barycenter set to zero. The galaxies appear highly elliptical with this kind of measurement. However, the effect of the PSF on the shapes is also amplified.

We take the PSF and both its compoments to be normalized to unity, which makes for well behaved quadrupole moments p_{ij} of p. As for $P^{\rm sm}$, KSB find

$$P^{\rm sm}_{ij} = \frac{1}{T}\left(X_{ij} - e^{\rm obs}_{ij} x_i\right), \tag{2.13}$$

$$X_{ij} = \int \mathrm{d}^2\theta i(\theta)\left[\left(W + 2\theta^2\frac{W'}{\sigma^2}\right)\delta_{ij} + \eta_i(\theta)\eta_j(\theta)\frac{W''}{\sigma^4}\right], \tag{2.14}$$

$$x_i = \int \mathrm{d}^2\theta i(\theta)\eta_i(\theta)\left(\frac{2W'}{\sigma^2} + \theta^2\frac{W''}{\sigma^4}\right), \tag{2.15}$$

$$\eta_1 \equiv \theta_1^2 - \theta_2^2, \qquad \eta_2 \equiv 2\theta_1\theta_2, \tag{2.16}$$

where δ_{ij} is the Kronecker delta and the prime denotes differentiation with respect to θ^2.

The given quantities in these equations are the image i, the weight W. The measurable quantities are the weight extent σ, $e^{\rm obs}_i$, and the PSF anisotropy polarization p_i. Because gravitational lensing doesn't affect stars due to their largeness and proximity to Earth, and because stars are expected to be circular, any deviation from zero polarization arise only from PSF anisotropy. Using equation (2.11) for stars, which we denote with *, we determine p_i by measuring a star's polarization,

calculating its smear polarizability, and plugging into

$$p_i = (P^{*,\mathrm{sm}}_{ij})^{-1} e^{*,\mathrm{obs}}_j. \tag{2.17}$$

The final step in PSF deconvolution is to interpolate p_i across the field with a low order polynomial. Once this is done, we can determine how the PSF affects the source polarizations and correct for this to linear order.

2.1.4. *Estimate the shear.* Once we correct for the effects of an anisotropic PSF, we are left with the pure gravitationally lensed source polarizations e^γ_i, related to their hypothetical pre-lensed selves e^0_i by

$$e^\gamma_i = e^0_i + \delta e^\gamma_i \tag{2.18a}$$

$$= e^0_i + P^\gamma_{ij}\gamma_j. \tag{2.18b}$$

All quantities are defined in direct analogy to those of §2.1.3, except here we use γ to denote shear. For example, P^γ is the "shear polarizability" tensor that tells us the degree to which shear can affect a given source's polarization.

The expectation value of the true source polarizations $\langle e^0_i \rangle$ over a population is 0, so (2.18) provides an estimate of the shear γ in the image. In other words, we first choose some scale over which to average the corrected source ellipticities. In doing so we seek to include as many galaxies as possible in order to minimize counting errors while also maximizing the number of bins in the field. Finally, we solve for the shear after setting $\langle e^0_i \rangle = 0$.

In weak lensing analysis we wish to determine the convergence κ from (1.30), which is equal to the dimensionless sheet mass density in the field. The isotropic component of the PSF also affects a convergence in the image, which we must deconvolve beforehand. KSB do not provide the means to do so, so we must look elsewhere.

2.2. **RRG.** Rhodes, Refregier, and Groth [RRG] build on the KSB method, seeking to improve it's accuracy. As in the KSB method, they first measure the weighted, low order multipole moments of the sources and of the PSF. RRG also include one higher order term, namely the fourth order moment

$$I_{ijkl} \equiv \int \mathrm{d}^2\theta W(\theta^2/\sigma^2) i(\theta). \tag{2.19}$$

Also in contrast with the KSB method, RRG perform all calculations using the multipole moments themselves rather than the ellipticities. This may reduce the number of calculations, but at the same time RRG include many new steps in the source shape correction.

RRG first measure the distortion the camera itself causes in an image. How to proceed in this step depends on the particular instrument at hand. RRG use HST as an example, building on results arrived at by others who found HST camera distortions by inspecting images highly dense with stars. They find the perturbation this causes for the source polarizations to be less than a percent on average. This is small but nonetheless on the order of the shear signal we seek in weak lensing.

Next, RRG measure the weighted source multipole moments as already discussed. They parse the galaxy and the star sources, using the latter to determine the PSF. In the process of finding the PSF moments, they correct for the camera distortion, which they also do for the source moments.

Third, RRG correct for the anisotropic component of the PSF, then the isotropic component. The anisotropic correction is consistent with the KSB method, but RRG generalize by deriving an expression that corrects the fourth order terms as well.

Finally, after correcting for all distorting and convoluting effects, RRG arrive at the shear exactly as in §2.1.4.

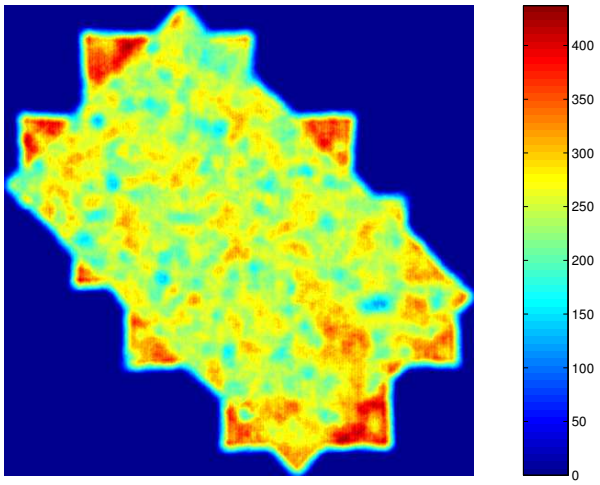

FIGURE 2. The smoothed density of sources found by Source Extractor in the GOODS HDF-N. This map clearly exhibits the effects of drizzling. The edges, where the fewest layers of stacked images are, contain considerable overdensities (red).

2.3. **Shapelets.** Refregier and Bacon [4] develop an entirely different approach to finding the weak lensing shear. At the heart of their method is the quantum harmonic oscillator basis—a complete, orthonormal set of basis functions consisting of Gaussian weighted Hermite polynomials.

In the Shapelets method we first decompose each source image into the coefficients of the two dimensional basis, which is essentially one integration per coefficient. As in the other two methods discussed, we parse stars and galaxies. Here, we project the stellar shapes onto the basis functions, attribute any deviations from circular shapes to the PSF, and interpolate the PSF across the field with low order polynomials. We then deconvolve the galaxy shapes using what Refregier and Bacon term the *convolution tensor*. To low order, deconvolution of the image at hand amounts to simple matrix operations involving the PSF kernel, the convolution tensor, and the source image itself.

Finally, we use the assumption, as before, that the expectation value of an ensemble of galaxy polarizations is zero to estimate the shear. Shear estimation reduces to matrix operations on the coefficients of each source.

3. OUR FINDINGS

We seek a weak lensing signal in the Great Observatories Origins Deep Survey, or GOODS. Our preliminary research proves educational while the data reveal the highly senstive nature of weak lensing measurements.

3.1. **GOODS.** GOODS consists of images taken by the Hubble Space Telescope in its "Deep Field North" (HDF-N), and the Chandra X-ray Observatory in its "Deep Field South" (CDF-S). These fields contain a minimal number of nearby obscurations such as stars in our own galaxy and are thus ideal for high redshift observation. GOODS is quite deep: some have reported galaxies in the field at redshift of six or so. On the other hand, GOODS is not particularly wide, as it covers about 320 arcmin^2 in its two disjoint fields. The combination of minimal stellar sources and a narrow field is a significant tradeoff to depth in light of weak lensing analysis.

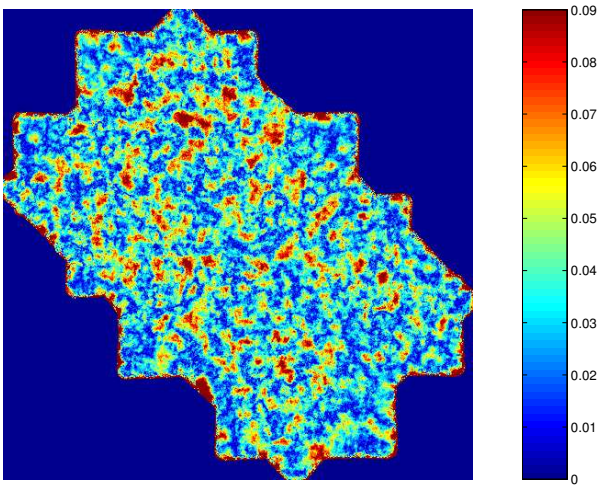

FIGURE 3. A shear map of the raw data. The shear can be decomposed into E and B modes, which provide a measure of the mass density and the systematic error in the field, respectively.

A second trade-off is GOODS's scheme of improving the resolution of the images. In their second data release, version 1.0, GOODS stack and drizzle thousands of raw images to construct a final mosaic. This has the potential to affect highly anisotropic errors in noise and galaxy shapes from position to position. The benefit, however, is improved resolution of 0.03 arcsec/pixel over the original 0.05 arcsec/pixel of the version 0.5 data. Our preliminary shape measurements and shear estimates confirm the presence of sizeable systematic error.

3.2. **Shape Measurements, Shear Estimates.** We have C++ software that calculates source polarizations in the GOODS data. We do this by measuring the quadrupole moments of each source. In preparing each source we apply circular apertures, which minimizes polarization biasing at $\pm 45°$ to the horizontal. We have experimented with a couple techniques to eliminate noise and mask neighboring sources. A comparison of some of these schemes is illustrated in Figure 1. This kind of experimentation in shape measurement has proven educational, but convolution with a well defined kernel such as a Gaussian will be essential to our weak lensing search.

In order to open our weak lensing data pipeline we have estimated the shear in the HDF-N, i-band as

$$\langle \gamma_i \rangle = \frac{\langle e_i \rangle}{2}, \tag{3.1}$$

which is simply Equation (2.18) for the impractical case of unity weight. The resultant shear map appears in Figure 3.2. Theory predicts weak lensing shear to be on the order of a few percent. The shear amplitude appearing in Figure 3.2 is considerably greater than the expected value. We attribute this high signal to systematic error in the field, which our shape measurement scheme have effectively amplified. This is illustrated in our decomposition of the shear into E and B modes, as suggested by Kamionkowsky et al. 1998 [3].

The E and B modes bring to light two aspects of the shear. First, the E mode of the shear is equal to the convergence, which in the limit of weak lensing is itself equal to the unitless sheet mass density κ from (1.30). Therefore, if we have performed effective image restoration and have a high enough density of sources, we then have a good estimate of the mass density in the field up to a constant. From this we can directly calculate the power spectrum of mass density perturbation and

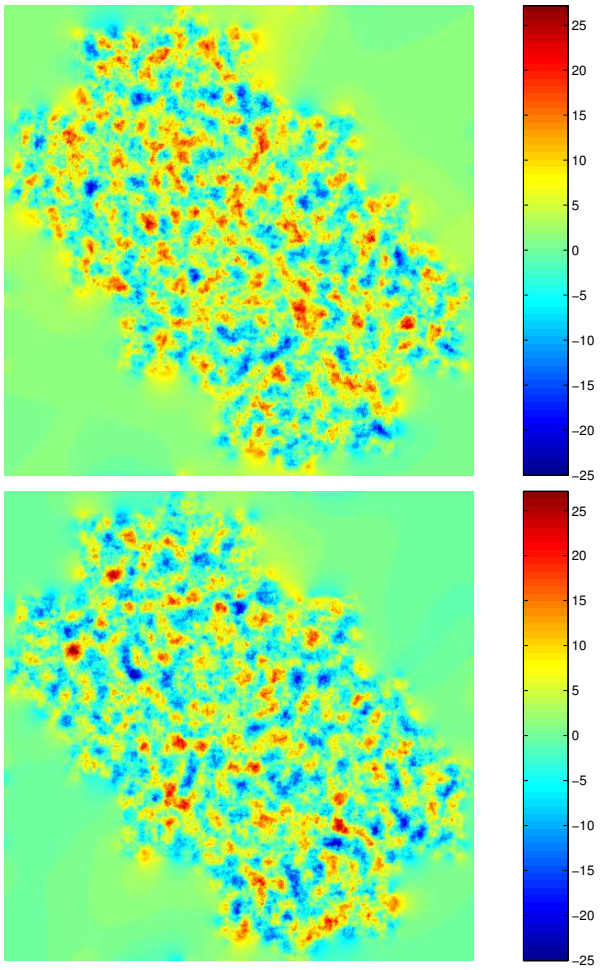

FIGURE 4. *Top*: An E mode map. This is equivalent to a normalized convergence map on the field, which, in the limit of weak gravitational lensing, equals the normalized and projected mass distribution. *Bottom*: A B mode, or curl, map. Theoretically, gravitational lensing gives rise only to E modes in the curl. B mode contributions from lensing are null or negligible. On the other hand, we assume that systematic error contributes to E and B modes equally. Because the above B mode map has amplitude on the order of our E mode map, we cannot trust that our E mode map accurately reflects the projected mass density in the sky.

its large scale normalization factor σ_8—fundamental quantities in cosmology. The top panel of Figure 4 shows our own E mode map, calculated from the shear map of Figure 3.2.

Second, the B mode signal provides a measure of the systematic error. Because weak lensing causes E modes almost exclusively, we expect B modes to arise only from camera distortions and PSF. Our B mode map in the bottom panel of Figure 4 exhibits signal amplitude on the order of the corresponding E mode map. Because of this, we cannot trust that our E mode map accurately reflects the projected mass density in the GOODS HDF-N. We must continue therefore to fine tune our shape measurements and to embark on distortion correction and PSF deconvolution.

3.3. **What's Next.** Our immediate next step is to apply a Gaussian weight to each source, with width σ equal to the extent of the source itself. Once we do so we will have completed our source shape measurement algorithm. Following that is the crucial process of PSF measurement and deconvolution. This will be particularly challenging using GOODS because of the low density of nearby stars. We will seek any such stars as well as explore the use of the HST PSF calculation software Tiny Tim as a means of finding the GOODS PSF.

Acknowledgements

I owe thanks to my advisor, Prof. George F. Smoot, for the opportunity to study weak lensing in GOODS under his tutelage, and to Dr. Jodi Lamoureux of Lawrence Berkeley National Laboratory for her guidance throughout the research. I thank Dr. Henk Hoekstra for some enlightening discussions.

References

[1] Blanford, R. D., Saust, A. B., Brainerd, T. G., & Villumsen, J. V. 1991, MNRAS, 251, 600.
[2] Hartle, J., *Gravity: An Introduction to Einstein's General Relativity*, 2003, Addison-Wesley.
[HFKS] Hoekstra, H., Franx, M., Kuijken, K., & Squires, G. 1998, ApJ, 504, 636.
[KSB] Kaiser, N., Squires, G., & Broadhurst, T. 1995, ApJ, 449, 460.
[3] Kamionkowski, M., Babul, A., Cress, C. M., Refregier, A. 1998, MNRAS, 301, 1064.
[4] Refregier, A., & Bacon, D. 2003, MNRAS, 338, 48R.
[RRG] Rhodes, J., Refregier, A., & Groth, E. 2000, ApJ, 536, 79.

Department of Physics, University of California, Berkeley
E-mail address: fwh@berkeley.edu
URL: http://www-astro.lbl.gov/~fwh/